Environmental Earth Sciences (2018) 77:414
https://doi.org/10.1007/s12665-018-7583-3

ORIGINAL ARTICLE

Developing an algorithm for automated geometric analysis and classification of landslides incorporating LiDAR-derived DEM

Saied Pirasteh[1] · **Jonathan Li**[2]

Received: 16 March 2017 / Accepted: 24 May 2018 / Published online: 1 June 2018

Abstract

Amending landslides inventories is immensely important to policy and decision makers alike. Sliding creates geometric shapes on the Earth's surface. This study presents the utilization of LiDAR high-resolution digital elevation model (DEM) in the Alborz Mountains, Iran to refurbish the existing landslide inventory dataset by implementing the proposed algorithm. The method consists of the automated derivation of landslide geometry (length, width, and area) followed by classification of landslide types considering length, width and flow direction. This study has used the trapezoidal rule for numerical integration to develop the proposed algorithm. The landslides were then classified into four types (very long, long, very wide, and wide) based on slope, length, and width. This geometric classification of landslides is based on the geographical coordinates, slope angle (θ), length (L), and width (W), and further failure flow direction. A total of 95 landslides were updated from the existing inventory database. The proposed method was verified and evaluated by field observations; and 14 samples were tested to determine the relative error. The results demonstrated that the mean percentage relative error is 0.496% in length and width and 0.008% in area, related to the GIS analysis. The accuracy performance of determining the landslide's type is 92%. The purposefulness of this algorithm is to increase the accuracy performance of landslides geometry analysis and automated measurements associated with the usual GIS platforms such as ArcGIS.

Keywords Landslide classification · Length · Width · Area · Computing techniques · Trapezoidal rule · LiDAR · Inventory map · MATLAB · Alborz Mountains

Introduction

Landslides, a natural hazards phenomenon, are common deformation scenarios on the Earth's surface. This geomorphic process is significant in developing the geometry of landslides and can be used to determine landslide typology (Wu and Sidle 1995; Wehr and Lohr 1999; Watts 2004; Wu et al. 2008; Westen et al. 2008; Hattanji and Moriwaki 2009; Niculiţă 2015, 2016; Shirzadi et al. 2017; Wen et al. 2017; Pirasteh 2018). Characterization of topography and morphology and classification of landslides requires knowledge of not only geologic and geomorphic processes and image interpretation, but also technologies such as LiDAR. In the last two decades, researchers have applied the high-resolution DEM derived from LiDAR point clouds to improve landslide delineation (Su and Stohr 2000; Barlow et al. 2003; Ali et al. 2003b; Zhou et al. 2003; Sherrod et al. 2004; Ali and Pirasteh 2004, Su and Bork 2006; Ardizzone et al. 2007; Teza et al. 2007; Tian et al. 2008; Travelletti et al. 2008; Pirasteh et al. 2009, 2011, 2017; Pradhan and Pirasteh 2010; Jaboyedoff et al. 2012; Zare et al. 2013; Lyons et al. 2014; Yousef et al. 2015; Pirasteh and Li 2016, 2017; Petschko et al. 2016; Gaidzik et al. 2017; Golovko et al. 2017). LiDAR-derived DEMs allow for the detailed exploration of morphology and geometry of landslides that could possibly be used for updating the landslide inventory (McKean and Roering 2003; Schulz William 2007; Petschko et al. 2016).

✉ Saied Pirasteh
s2pirast@uwaterloo.ca; moshaver1380@gmail.com

Jonathan Li
junli@uwaterloo.ca

[1] Environment 1-401A, Department of Geography and Environmental Management, Faculty of Environment, University of Waterloo, 200 University Avenue West, Waterloo, ON N2L 3G1, Canada

[2] Environment 1-111, Department of Geography and Environmental Management, Faculty of Environment, University of Waterloo, 200 University Avenue West, Waterloo, ON N2L 3G1, Canada

A landslide inventory contains a collection of polygon shapes, types, lengths, widths, areas, locations, and other information related to landslides. With such information, landslides can be represented digitally in the GIS environment either manually of semi-automatically (Freeman 1991; Ali et al. 2003a; Malamud et al. 2004; Martha et al. 2010; Lyons et al. 2014). Landslide inventory and spatial analysis have played a significant role for decision makers in preparing a loss-reduction plan as well as in establishing an early warning system. However, few studies have focused on the development of automated algorithms for geometry characterization and landslide classification (Ardizzone et al. 2002; Malamud et al. 2004; Mondini et al. 2011; Lyons et al. 2014; Niculiţă 2015, 2016). Characterization of landslide geometry depends upon various factors. For this reason, classification of landslides has been based on different discriminating factors and is therefore at times very subjective (Varnes 1978; Hutchinson 1988; Cruden 1991; Dikau et al. 1996). However, some researchers have abstracted the shapes of the landslide to a rectangle to define the long side (i.e., length) and short side (width), instead of the factual shape of a landslide. The length of a landslide is defined as the length of the line from the crest to the end of the toe in the failure direction of a landslide area. The landslides are then classified based as either a long or a wide type upon the geometry (length and width) of the defined rectangle that covers the landslide (Niculiţă 2016). Moreover, most researchers have considered the failure direction as the length of a landslide with respect to engineering geology and have dealt with vector system, three-dimension, and dynamic system. Therefore, the failure direction is defining the length of a landslide. Although Taylor and Malamud (2012) assumed that all landslide shapes can be abstracted to a rectangle to define the long side [i.e., length (*L*)] and short side [width (*W*)] (Fig. 1), previous researchers developed semi-automated tools to measure the length and width of landslide polygons (Ardizzone et al. 2002; Malamud et al. 2004; Yimaz 2010; Mondini et al. 2011; Lyons et al. 2014; Taylor et al. 2015; Niculiţă 2016).

In contrast, this study has used the numerical integral trapezoidal rule (NITR) to develop an algorithm for automated landslide geometric analysis and classification (Burden and Faires 2011). The proposed approach includes determination and measurement of the length, width, and area; as well as the identification of the landslide type. The 2D scalar system for characterization of the landslide geometry is applied regardless of the failure direction, type of materials, and speed of movement and type of materials.

This paper presented the proposed approach to automated landslide detection through determining the length, width, area, and type of landslide in a 2D, scalar, and static-based polygon covering the factual shape of the landslide. The approach is utilized to update the landslide inventory in the Alborz Mountains, Iran, where typical geomorphologic features and various shapes of landslides exist. The 2D scalar static system is based on the projected geographic coordinates system for representing the slope angle, length, and width of landslide polygons. The slope angle, which is the angle of the segment with respect to *X*-axis, is not a topographic slope. The LiDAR-derived DEMs along with field observations and remotely sensed images are used to support on screen manual digitization of landslide polygon in GIS environment and to update the landslide inventory.

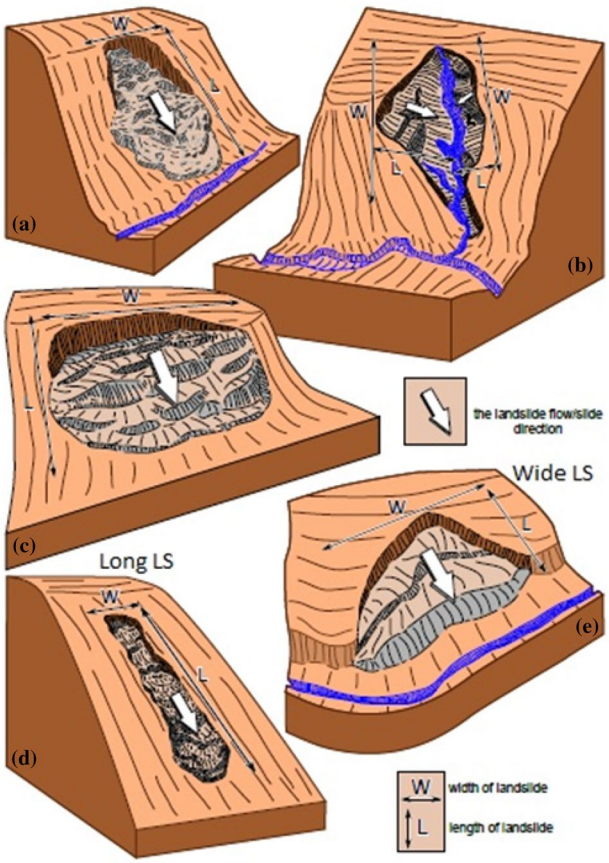

Fig. 1 Schematic drawings of long and wide cases of landslides with *X*-axis and *Y*-axis: **a** rotational slide—long type, **b** gully bank slides—long type, **c** translational slide-wide type, **d** flow—long type, and **e** river bank slide—wide type. (Source: Niculiţă 2016)

The study area

The Alborz Mountains of Mazandaran Province in the north of Iran are parts of the Alpine-Himalayan system. The study area (Fig. 2) is located in the Central Alborz and from the north reaches to the Caspian Sea, and from the south–southwest goes to Tehran. It locates between 445438.111E–624039.018E and

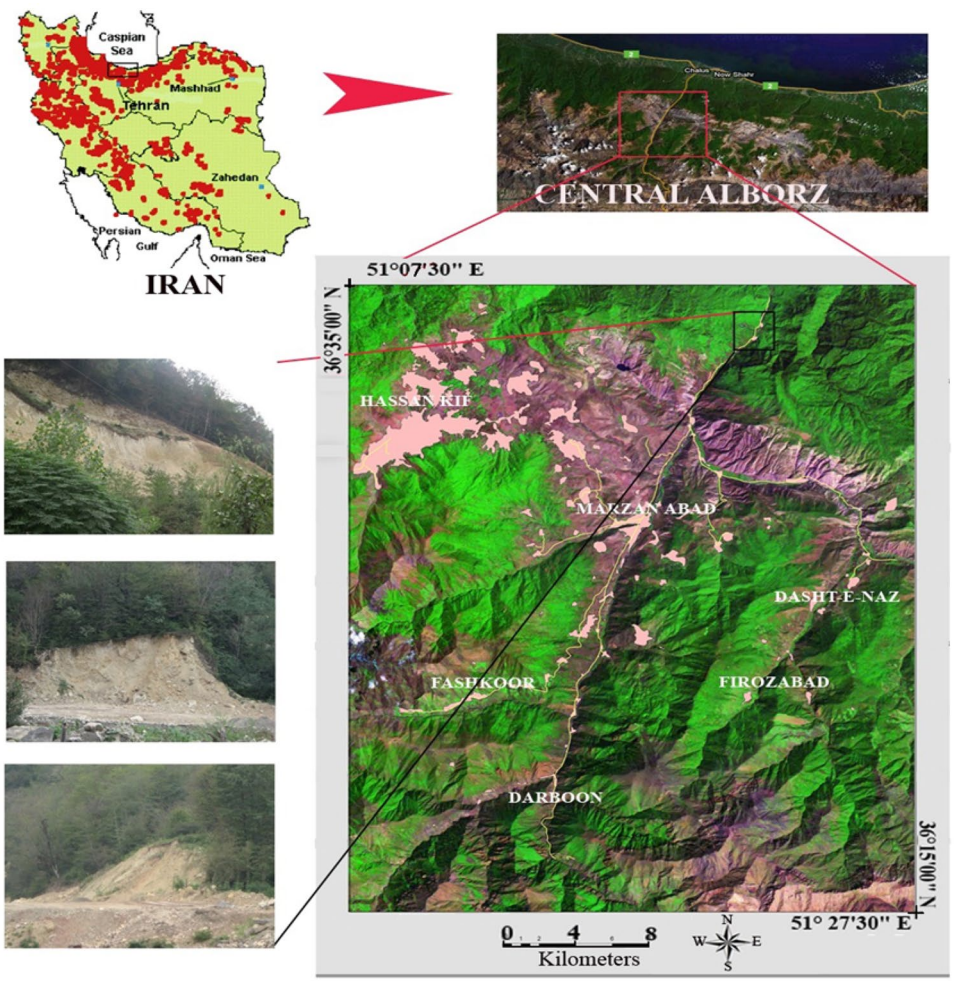

Fig. 2 Study area

4071833.357N–3970631.884N in UTM. The elevation of the study area varies between 92 and 5590 m from the mean sea level (MSL). The annual precipitation is above 1000 mm, and seismically the study area is active and triggers landslides. The updated inventory dataset contains 95 landslides with minimum and maximum length of 5–900 m, respectively. The width of landslides varies from 8 to 800 m, and the area of landslides is from 9 to 610,000 m^2. Various reasons such as high topography, seismicity, high precipitation, the resistance of rock types, tectonic geomorphology, and slopes have caused landslides such as transitional, rotational, compound flows, and rockfalls (Hungr et al. 2014).

Data process and method

The landslide inventory archives of the Alborz Mountains, Mazandaran Province (Fig. 2) and Google Earth images (dated in December of 2009, 2010, 2011, 2012, 2013, 2014, 2015, and 2016) were used together in the present study for the analysis with the 5 m resolution LiDAR-derived DEMs. The Real Time Kinematic (RTK) Global Positioning System (GPS) SmartNet was also used during field observations to enable digital drawing of landslide polygons in ArcGIS using ArcBruTile tool. There are complex landslides and a single event in the inventory database of the study area. This landslide inventory contains 173 points and polygons representing landslides small to large in length, width, and area. To update the landslide inventory and to test the performance of the proposed algorithm, 20 cm resolution unmanned aerial vehicle (UAV) images covering the Chalus District in the study area were also used and; integrated with the Airborne LiDAR point clouds with point spacing of 20 cm (Fig. 3) to support on screen manual digitization of landslide polygon in GIS environment. A total of 95 landslides were selected from the landslide inventory database to convert points into polygons based on screen manual digitization of the landslide polygon in GIS environment using visual image interpretation techniques of high-resolution of UAV, Google Earth images as well as LiDAR-derived DEM; 14 samples were used to test the proposed algorithm.

Materials move towards downslope, and the distance of the mass displacement in a landslide is usually greater than the width of the displaced material. This occurs especially

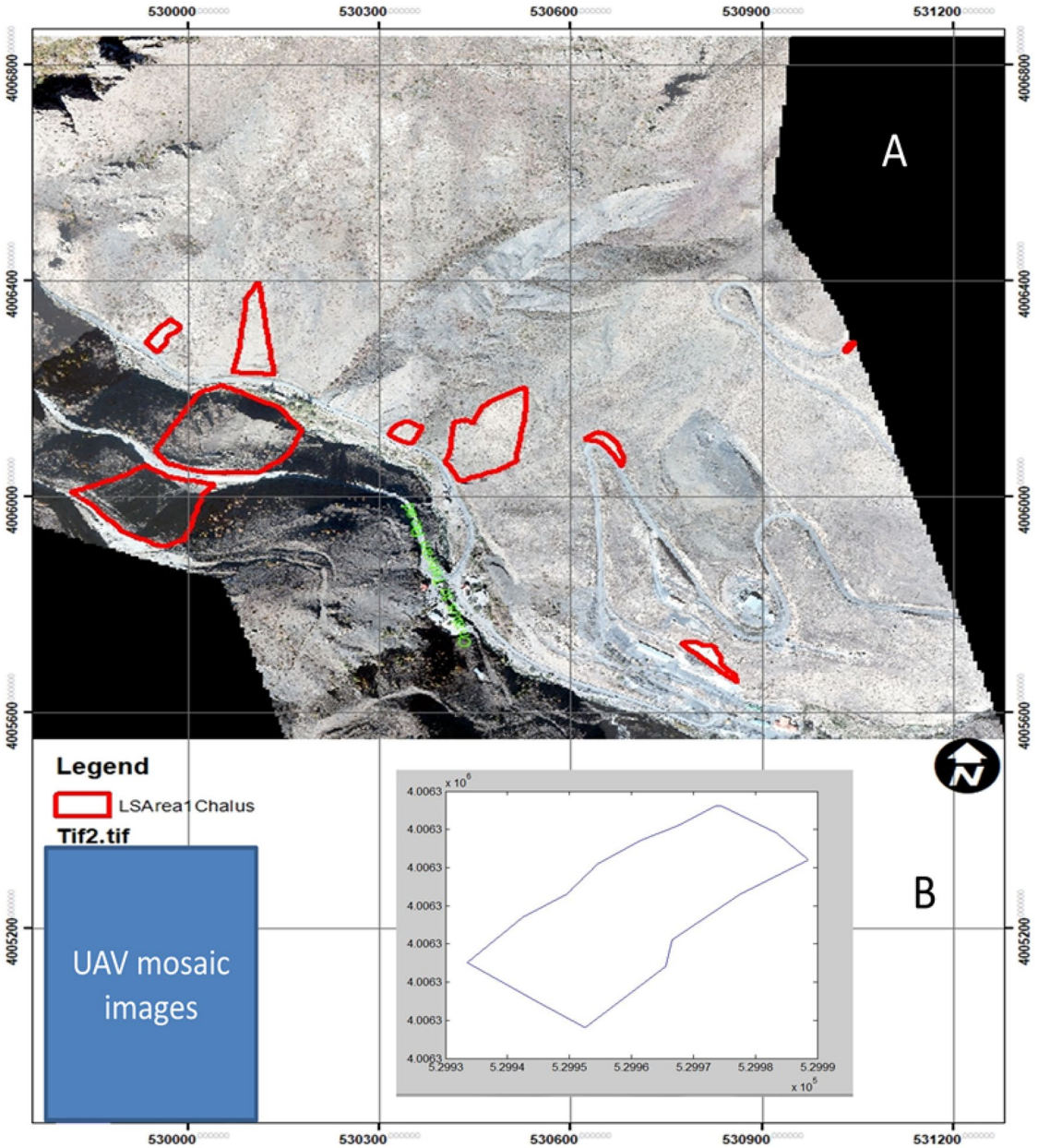

Fig. 3 **a** Landslide polygons and UAV images, **b** selected landslide polygon in the proposed software package. Location: Chalus District

for flows, but also for the majority of slides, and it means that the length is greater than the width ($L > W$). In some landslides, this phenomenon does not happen and we might have a smaller length than width ($L < W$). In the proposed method, the maximum distance of two points (i.e., the longest segment) in either X-axis or Y-axis in the 2D scalar system is taken into account to discern the length and width of a landslide and to define the landslide type. The following section details the proposed methodology.

In engineering geology, the length of a landslide is defined as the length of the line from the crest to the end of the toe in the failure direction of a landslide area. However, the proposed approach assumes that a landslide polygon can be represented in a 2D static scalar system when required, instead of considering the failure direction as the length of the landslide to be represented in a 3D dynamic vector system. As such, landslide length, width, area, and type can be applied for determining the landslide geometry regardless of the failure direction, speed of materials movement, type of materials, and type of materials movement (Varnes 1978; Picke 1988; Cruden 1991).

Nevertheless, the following paragraph summarizes how the proposed algorithm and method work.

To determine a landslide type, the proposed algorithm and code runs searching process to determine highest and lowest points on the polygon with many iterations until it identifies the highest and lowest point of that particular polygon. The algorithm is designed and scripted in such a way that it considers the failure flow direction and slope down materials if analysts required. If not, an analyst can follow the 2D scalar static concept that means it works only with one digital elevation model (DEM) or *x, y, z* dataset of a landslide polygon in conjunction with considering the defined failure flow direction. The analyst can also use the 3D vector dynamic concept that means the proposed algorithm and code can run with additional scripts to consider DEMs of before and after a landslide, if data are available. However, the longest segment concerning the failure flow direction will be the length of a landslide. A perpendicular line concerning determining the highest and lowest point from the same polygon to the length of the landslide will be the width of the landslide. In addition to the above, the classification of a landslide polygon is based on the geographical coordinates, slope angle (θ), length (L), and width (W), and further failure flow direction. The following steps are considered when writing the code for developing the automated or semi-automated extraction of a landslide geometry:

(a) Input data;
(b) Find maximum and minimum X and Y with respect to the failure flow direction;
(c) Calculate $d_1 = (l_1)$ and $d_2 = (w_1)$ and their slopes with angle;
(d) Determine a landslide type;
(e) For a wide landslide, recognize top and bottom points and sort them into two separate matrices;
(f) Calculate the area under the top and bottom curves;
(g) Identify, measure, and determine width (Alpha angle between length and width);
(h) Calculate area and print output (type, length, width, and area);
(i) For a long landslide, recognize right and left points and sort them into two separate matrices;
(j) Calculate the area under right and left curves;
(k) Identify, measure, and determine width (Alpha angle between length and width); and
(l) Calculate area and print output (type, length, width, and area).

Numerical integral trapezoidal rule (NITR)

In this study, the trapezoidal rule was used to analyze landslide geometry and to classify landslides. The trapezoidal rule is a numerical analysis method that has been applied to approximate the value of a definite integral (Burden and Faires 2011; Zhao and Zhang 2014). The integral is approximated using n trapezoids formed by straight line segments between the points $(x_i - 1,\ y_i - 1)$ and $(x_i,\ y_i)$, for $1 \le i \le n$, as shown in Fig. 4. Each trapezoid in a landslide polygon is calculated by:

$$\int_a^b f(x)\mathrm{d}x \approx \frac{\Delta x}{2}(y_0 + 2y_1 + 2y_2 + \cdots + 2y_{n-1} + y_n). \quad (1)$$

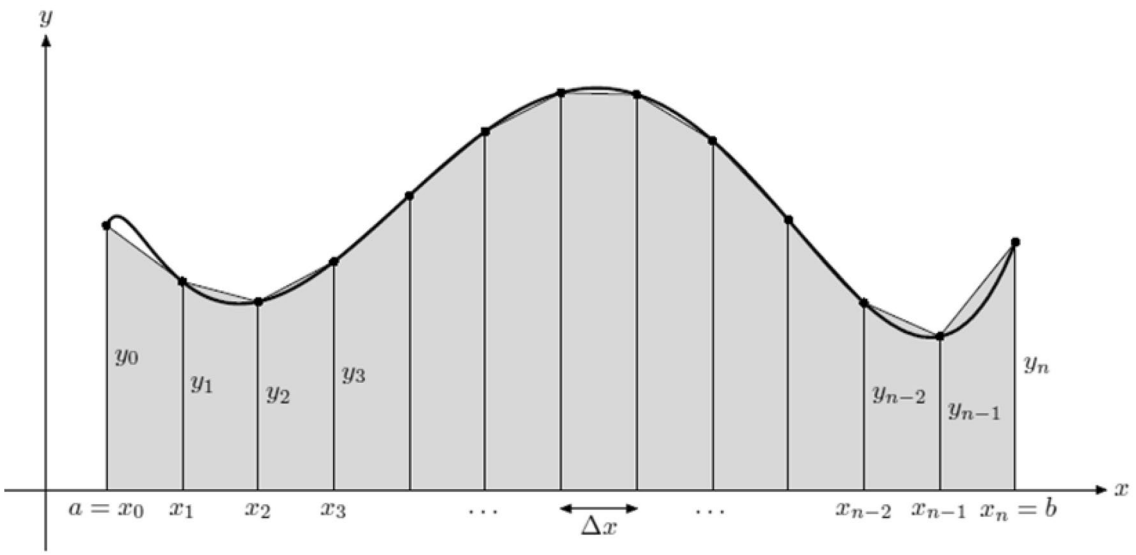

Fig. 4 Each trapezoid is shown in a landslide polygon

The NITR method was coded by matrix-based MATLAB language in several lines to run the computational process of a landslide and to determine the length, width, area, and type of landslide. The script code is available at http://www.widm.ca upon request.

In this study, RTK SmartNet with 14–20 cm accuracy was used in ground truthing to collect ground control points (GCPs) for simulating landslide polygons. Then, the polygons were created both in the GIS platform using the measurement tools (Fig. 5) and in the proposed algorithm to calculate the length, width, and area and to identify the landslide of the polygons. This study used ArcGIS 10.4 version to determine the boundary' points of a landslide polygon by moving curser manually on the screen visualization to identify the coordinates of each point on the polygon. The coordinates of each selected point was recorded in Excel that is to be used further in the proposed algorithm and MATLAB. Later, the points in Excel with geographical coordinate system (*x, y*) were introduced to GIS platform and the proposed algorithm to draw the polygon and to calculate the geometry of the polygon.

The proposed algorithm was tested and verified by ArcGIS platform and field observations as well. However, the GIS and other platforms are possibly not available to determine the length and width of a landslide automatically, and to classify landslide types automatically as well. In contrast, the proposed algorithm package performs these functions automatically. The following figure describes the procedures of automated computation of the landslide geometry and classification.

Geometric analysis and rules of classification

In the Alborz Mountains, variable shapes of landslides cause uncertainty in determining the length, width, area, and landslide type of a polygon. Instead of using the existing methods, this study develops automated computing approach to landslide geometry by taking advantage of LiDAR-derived DEMs, Google Earth images, and UAV images for analyzing available landslides in the study area. The boundary of a landslide was determined by visual on screen digitization on the Google Earth and UAV images using image element techniques that are supported by field observations and inventory data.

To perform the automated calculation of segments in landslide polygons in this study, the rectangular coordinate system has the *X*-axis coincide with the east west direction and the *Y*-axis coincide with the north–south direction, in which the *x*-coordinates are referred to as latitude/northing and the *y*-coordinates are referred to as longitude/easting in the UTM with unit of meters (see Fig. 6). Polygons were converted to points using theArcGIS to measure the length and width. These points were then introduced to the proposed algorithm as attributing data in a table containing *x*- and *y*-coordinates. The following steps describe the procedure of computing length, width, and area by the proposed algorithm.

Step 1 To determine the X_{max} (A) and X_{min} (B) as well as Y_{max} (C) and Y_{min} (D) (Fig. 6) in scalar system. Points $A(X_{max}, Y_{Xmax})$, $B(X_{min}, Y_{Xmin})$, $C(X_{Ymax}, Y_{max})$, and $D(X_{Ymin}, Y_{min})$ are in the geographical coordinates system. The segment between points A and B is "d_1" and the segment between points C and D is "d_2". The d_1 is always in the favor of the *X*-axis and is considered to be x-coordinate or Latitude/Northing (m).

Step 2 To calculate AB(d_1) and CD (d_2) using the following equations:

$$\mathrm{AB} = d_1 = \sqrt{(X_{max} - X_{min})^2 + (Y_{Xmax} - Y_{Xmin})^2}, \quad (2)$$

$$\mathrm{CD} = d_2 = \sqrt{(X_{Ymax} - X_{Ymin})^2 + (Y_{max} - Y_{min})^2}. \quad (3)$$

Step 3 To compare d_1 and d_2 and to determine which landslides are classified into long types or wide types. The following section describes the next step and explains

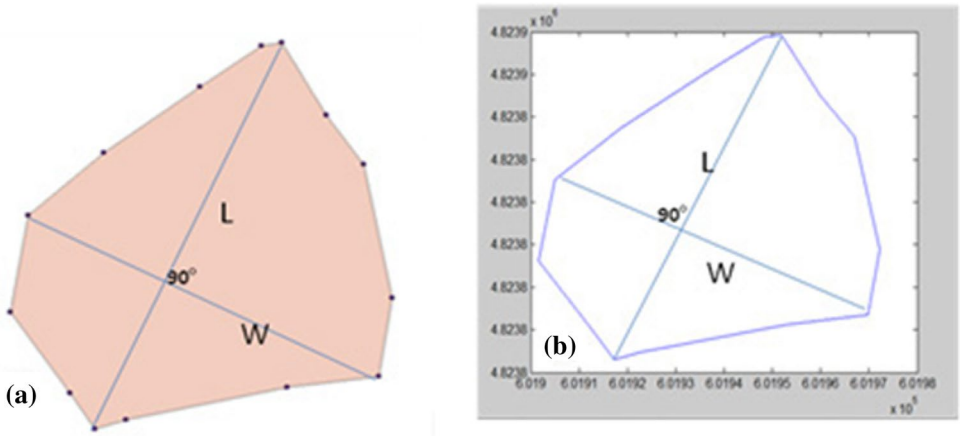

Fig. 5 **a** A polygon in ArcGIS. **b** The same polygon in the proposed software package

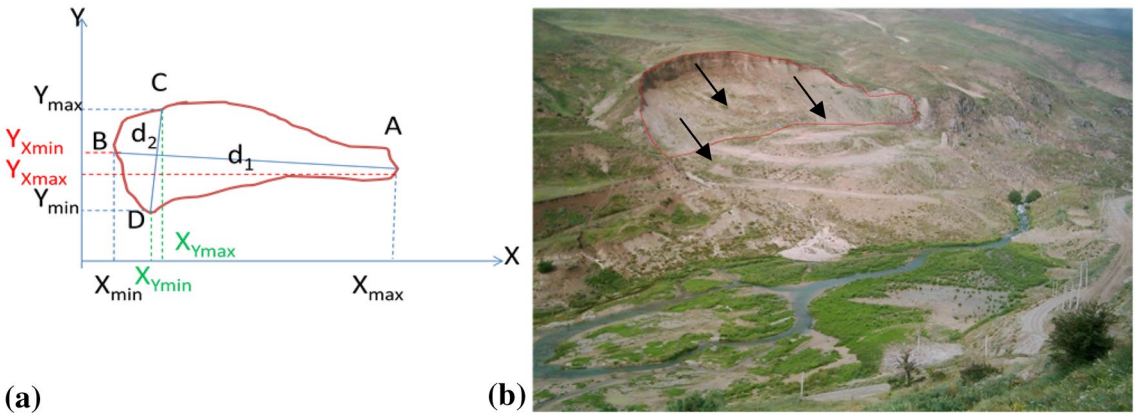

Fig. 6 **a** A wide type landslide polygon in the x–y coordinate system. **b** Photo taken during the field observation in the study area. Location: Imam Zadeh Hasan, Mazandaran Province

how this study classifies landslides based on the geometric features.

Furthermore, the automated classification of landslides was carried out in this study. Landslides were classified upon the $d_1$and $d_2$values with respect to the *x*- and *y*-coordinates as well as the slope angle (θ). Geometrically, the maximum distance between the two points can define the type of landslide aligning along either the *X*-axis or the *Y*-axis. If d_1 is larger than d_2, then the landslide polygon will be classified as the wide type and d_1 will be the "length" of the landslide polygon. If d_1 is smaller than d_2, then the landslide polygon will be classified as the long type. Figure 7 depicts the conceptual flowchart of the proposed landslide classification algorithm. This algorithm calculates both the maximum and minimum *x*-coordinates and *y*-coordinates of the landslide polygon. The maximum segment distance along the *X*-axis is determined the long side of the polygon, while the maximum segment distance along the *Y*-axis is determined the short side of the polygon. The algorithm also figures out these two distances. In other words, the algorithm computes the maximum and minimum Latitude/Northing (m) coordinates of points (*x,y*) from the landslide polygon in favor of the *X*-axis to estimate the "maximum horizontal segment distance". It also computes the maximum and minimum Longitude/Easting (m) coordinates of points coinciding with the *Y*-axis from the landslide polygon to estimate the "maximum vertical segment distance". The algorithm compares the maximum horizontal and vertical segments distance.

Following the previous steps, the fourth stage considers the amount of the slope angle (θ) to sub-classify landslides (Table 1).

To classify a landslide based on the proposed algorithm, long segment (d_1) length, angle of slope with respect to *x*-axis, and failure direction were considered. The side which is close to horizontal is considered to be very wide and as it gets close to vertical is very long. The selection of degrees in angle is based on bisector angle (i.e., equal angle) and of division in angle between 0° and 90°.

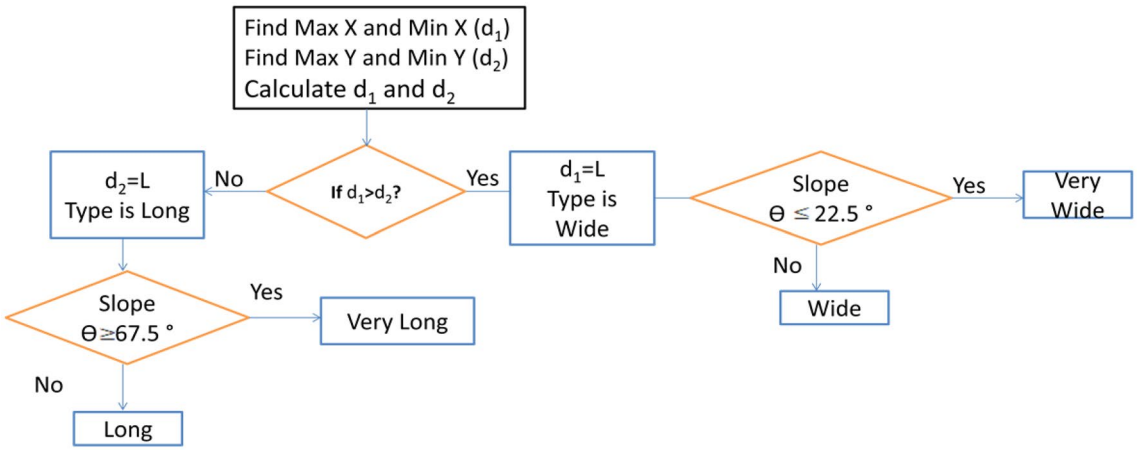

Fig. 7 Flowchart of the proposed landslide classification method

Table 1 Classification of landslides by the proposed method

Type of landslide	Slope angle (θ)
Long	$90° \geq LS > 67.5°$
Very long	$67.5° \geq LS > 45°$
Wide	$45° \geq LS > 22.5°$
Very wide	$22.5° \geq LS > 0°$

The slope angles can be calculated by:

$$\text{Slope } L = \frac{(Y_{X_{\max}} - Y_{X_{\min}})}{(X_{\max} - X_{\min})}, \tag{4}$$

$$\text{Slope } W = \frac{(Y_{\max} - Y_{\min})}{(X_{Y_{\max}} - X_{Y_{\min}})}, \tag{5}$$

where L is the length and W is the width of a landslide polygon (see lines 38 and 39 of the code).

The slope is always defined as $\Delta y/\Delta x$. Slope L describes the drawn segment slope between $X_{\max}$ and $X_{\min}$ in scalar 2D static system and slope W describes the slope of a drawn segment between two points that are with maximum y and minimum y.

Step 4 This step aims to determine the slope angle (θ) to sub-classify landslides (Table 1). The slope angle (θ), which is the angle of the segment with respect to X-axis, is not a topographical slope. If the slope angle (θ) is below 45°, then the landslide is classified as the wide type. If the slope angle (θ) is above or equal to 45°, then the landslide is classified as the long type (Table 1). For wide type landslides, there are two possibilities: (1) If the slope angle (θ) is below or equal to 22.5°, then the proposed algorithm identifies the landslide as the very wide type; or (2) If the slope angle (θ) is above 22.5° but below or equal to 45°, then the landslide is classified as the wide type. For long type landslides, there are two possibilities: (1) If the slope angle (θ) is above 45° but below or equal to 67.5°, then the landslide is classified as the long type; or (2) If the slope angle (θ) is above 67.5° but below or equal to 90°, then the landslide is classified as the very long type. The upper and lower limits of the slope angle depend on the x- and y-coordinates (Fig. 8). In this study, the classification of landslides into the very wide type (0°–22.5°), very long type (67.5°–90°), wide type (22.5°–45°), and long type (45°–67.5°) was dependent on the angle indicating the inclination of a landslide to either x-axis or y-axis. In other words, the upper and lower limits of slope angle for the landslide classification rely on each section of the 2D space. xoy (Fig. 8) has an angle of 90° between each axis. Because the bisector in each region is 45°, the criterion of this angle is the middle limit of 45° and it is evaluated by the proposed algorithm. Notably, this

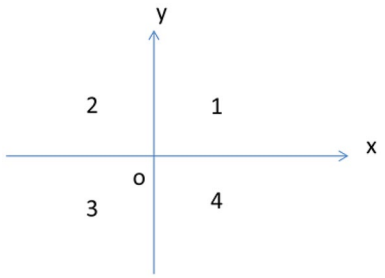

Fig. 8 Each section of the 2D space of xoy

study implemented the scalar system to run the process. However, it is not important in which region of the Cartesian coordinate system a landslide polygon falls in. Also, in classification of "very wide (0°–22.5°) or long (67.5°–90°)" and "wide (22.5°–45°) or long (45°–67.5°)", the criteria was the angle between the bisector to x-axis/y-axis, because this angle defines the closeness to the x-axis or y-axis which indicates the inclination of a landslide to either the x-axis or the y-axis (see code lines 38 and 39). The code is available upon request at s2pirast@uwaterloo.ca.

The final stage calculates the width and identifies the length of the landslide. Therefore, for determining d_1, d_2, the semi-automated calculation of length and width was created. In this study, the landslide geometry was determined in the 2D scalar system where the maximum distance between points (i.e., longest length of a segment) in a landslide polygon was considered. The proposed algorithm calculates and compares d_1 and d_2. The d_1 is the length of the landslide if $d_1 > d_2$, or the width of the landslide if $d_1 < d_2$. The algorithm can determine the longest segment when d_1 is perpendicular to d_2 (Fig. 9).

Automated calculation of area

Studying and classification of the shapes of landslide geometry are at times highly subjective. In the Alborz Mountains, landslides' shapes may be regular or irregular, which causes uncertainty in determining the length, width, area, volume, and type of landslide polygon. The geometry of landslides can be computed using different methods (Ghuffar et al. 2013; Pirasteh et al. 2015; Niculiťa 2016) and tools such as ArcGIS (http://support.esri.com/technical-article/000006109). This study used geodata analytical computing and NITR to improve the precision of the measurement of landslide polygons extracted from LiDAR-derived DEMs, Google Earth images, UAV images using visual image interpretation of photographic and geotechnical elements such as texture, shape, vegetation, and slope, and the available landslide inventory dataset.

To perform automated calculation of area, the proposed algorithm computes maximum and minimum projected

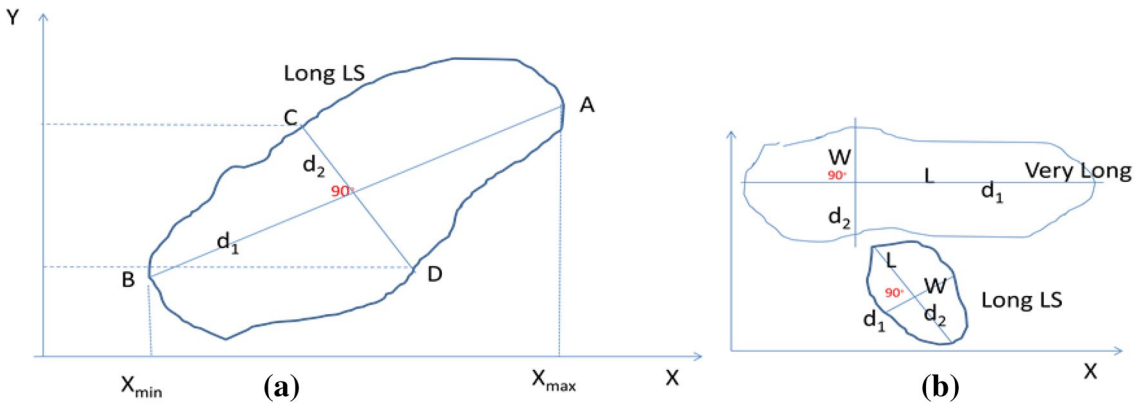

Fig. 9 **a** The longest segment of the landslide polygon. **b** Wide type and long type of landslides

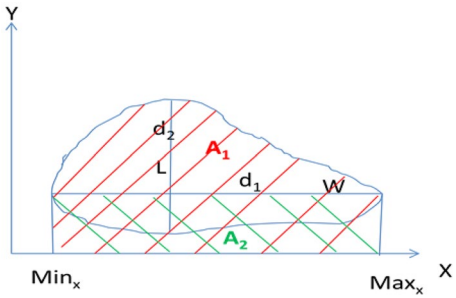

Fig. 10 Schematic of a wide type landslide

geographical coordinates of points (Easting and Northing) of a polygon boundary from the input data in the scalar. Next, a line (long side segment) is stretched between the maximum and minimum values of the polygon predisposed in x-coordinate. If a landslide is a "Wide" type, then a curve is drawn above the line to coincide with the *x*-axis. The curve above the line is called "Top Curve" (A_1). Also, the points under the line (long side segment) create another curve which is called a "Bottom Curve" (A_2). The area below the stretched line (i.e., Bottom Curve) is computed using the NITR formula. The same process is followed for the "Bottom Curve" and the area under the line is computed. Then, the system begins to subtract the area of the top and bottom curves. The area of the polygon is calculated as follows (Fig. 10):

$$A_p = A_1 - A_2. \tag{6}$$

If a landslide is a "Long" type, then the polygon is divided into "Left Curve" and "Right Curve" coinciding with the *Y*-axis; and the area of "Right Curve" and "Left Curve" are computed separately. Therefore, the system begins to subtract the area of "Right Curve" and "Left Curve", and the area of the polygon is computed (Fig. 11).

Use of LiDAR-DEM, UAV, and updating inventory dataset

In this study, 5 m resolution LiDAR-derived DEM was generated and represented in ArcGIS. The generated DEM derivatives such as slope were used to assist landslide classification along with field observations, UAV images, and Google Earth images.

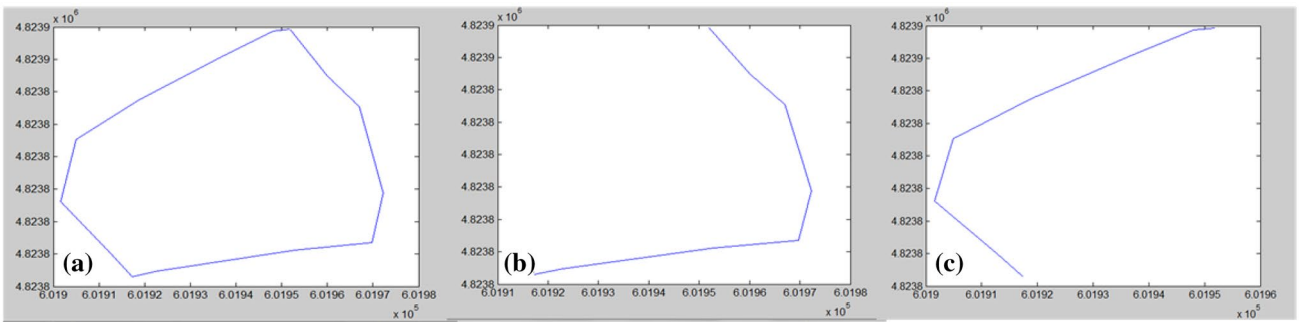

Fig. 11 **a** A polygon sketched using the proposed model, **b** "Right Curve", and **c** "Left Curve"

The raw LiDAR point clouds were first converted into the LAS format. LiDAR-derived DEM was used in ArcGIS to be integrated with the existing inventory datasets, while Google Earth images were used for better visual interpretation of landslides. In addition, 20 cm resolution UAV images covering Chalus District were used together with some field observations (Fig. 12) to identify new landslides, test the proposed algorithm, and update the landslide inventory map of the study area. Only some landslide polygons from the inventory database containing a total of 173 landslides were selected to test the proposed method. These polygons were converted into the points with *x*- and *y*-coordinates. These *x*- and *y*-coordinates were used to measure the long and short sides of the landslide polygon as well as to determine the landslide length, width, area, and type.

Validation

The performance of the algorithm was verified in ArcGIS and field observations in conjunction with the inventory dataset. The validation against the type of landslide was performed using the landslide inventory dataset of the particular study area of Chalus. Fifty-eight landslide polygons were selected from the study area for mapping. Fourteen actual and simulated polygons were selected to test the proposed algorithm on determining and measuring the length and width. Twenty-five landslides were also selected from the landslide inventory dataset to determine the accuracy of extracted landslide's type by the proposed algorithm (Table 2). The logic behind figuring out the width, length and area with the ArcGIS and the proposed algorithm in conjunction to the field observation measurements, and the inventory dataset is to check the relative error percentage and the reliability and accuracy of the proposed algorithm.

Table 2 Landslide's type validation

No. of selected landslides	Landslide in inventory dataset	Landslide in proposed algorithm	Accuracy (%)
25	Known	Extracted in this study	96

A polygon was selected and calculated in ArcGIS and in the developed algorithm using MATLAB, respectively. Other landslide polygons were also calculated in ArcGIS, ground truth (Fig. 12), and in the MATLAB by applying the developed algorithm, respectively, for the algorithm performance and relative error analysis. The proposed method was verified using field observations, measurement tools, and the Real Time Kinematic (RTK) SmartNet system in ground truth (Fig. 13). Basically, the RTK technique is used to collect points with *x,y,z* and to measure the length and width of the segment on the ground truth for further geometric analysis in ArcGIS as well as the proposed algorithm. RTK satellite navigation is a technique that has been used in this study to enhance the precision of landslide position data during ground truth measurement for simulation of the model. This RTK has derived from satellite-based positioning systems (global navigation satellite systems, GNSS) such as GPS. The percentage relative error was calculated by Kreyszig et al. (2011).

$$\text{Relative error}\% = \left[\left| L_{\text{ArcGIS or ground measurement}} - L_{\text{proposed software}} \right| / A_{\text{ArcGIS}} \right] \times 100, \tag{7}$$

$$\text{Relative error}\% = \left[\left| W_{\text{ArcGIS or ground measurement}} - W_{\text{proposed software}} \right| / A_{\text{ArcGIS}} \right] \times 100. \tag{8}$$

Fig. 12 Field photo of a long type landslide in Haraz District, Mazandaran Province

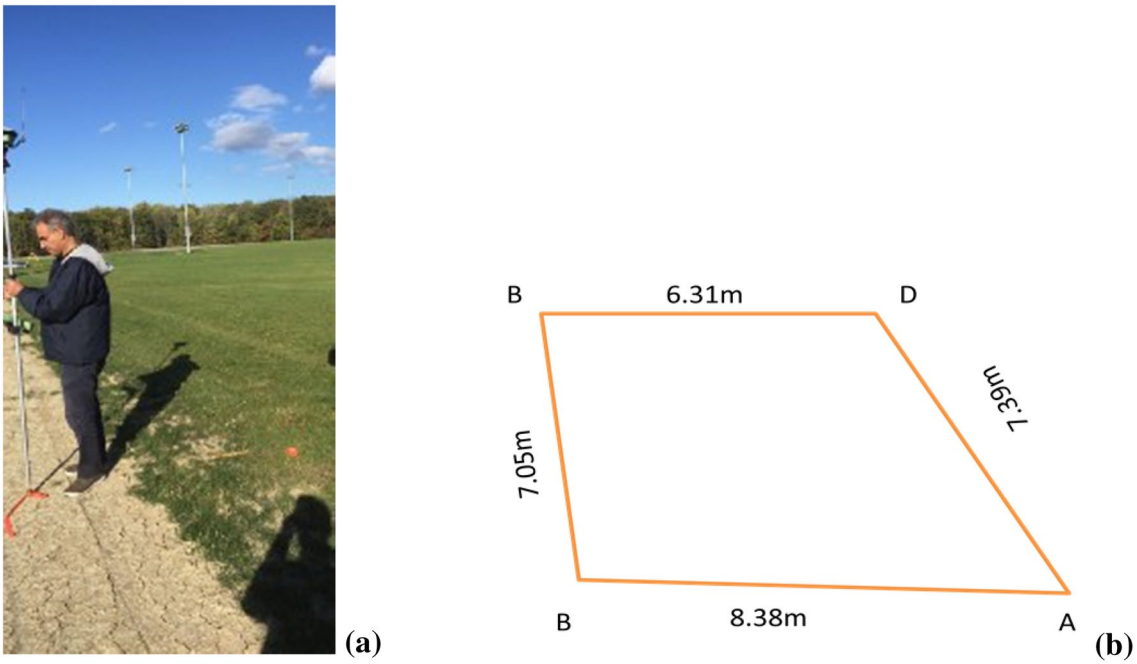

Fig. 13 **a** Ground truth measurement using RTK system, **b** schematic of a simulated polygon on the ground

Results and discussion

The results of this study form a response to the previous studies attempted by Taylor and Malamud (2012) and Niculiţă (2016). This study presented automatic landslide length and width extraction based on the NITR geometric processing of the landslide polygon and the geomorphometric analysis of LiDAR-derived DEMs.

The results of this study demonstrated that the proposed algorithm was able to automatically simulate, model, and determine the landslide length, width, and type which probably shows a promising approach in contrast to the existing GIS platform and algorithm delivered by Booth et al. (2009) and Niculiţă (2016). Both the long side and the short side of the landslide polygon can be measured automatically and the type of the landslide can be classified with the proposed method at an acceptable level. This investigation classified landslides into (a) long, (b) very long, (c) wide, and (d) very wide.

This study shows that the accuracy performance of the extracted landslide's type is 96% (Table 2) when the author implemented the proposed algorithm for twenty-five selected and tested landslides from the landslide inventory dataset. Table 3 depicts the measurement and relative percentage error with ArcGIS and the proposed algorithm. The dimensions of one of the selected polygon samples are 83.74 m in length and 69.30 m in width in ArcGIS, and 83.75 m in length and 69.31 m in width in the proposed algorithm in MATLAB, respectively. The calculated area of the selected polygon in ArcGIS is 3606.7 m^2, in comparison with 3606.4 m^2 in the proposed algorithm, respectively. The percentage relative errors were obtained = 0.496% in length and width, and 0.008% in area when using the proposed algorithm(Table 3a). Also, Table 3b depicts another example of the comparative measurement and relative percentage error with ArcGIS and the proposed algorithm.

Table 3 Measurement and relative percentage error

Geometry	ArcGIS	Proposed algorithm	Relative error (%)
(a)			
Length	83.74 m	83.75 m	0.01
Width	69.30 m	69.31 m	0.01
Area	3606.7 m^2	3606.4 m^2	0.008
(b)			
Length	113.12 m	113.46 m	0.30
Width	101.34 m	99.64 m	1.67
Area	6976.91 m^2	6988.20 m^2	0.16

Also, the relative percentage error of measurement of a tested landslide length and width of the polygon is 0.011 and 0.011, respectively (i.e., the proposed algorithm in MATLAB vs. ArcGIS) (Fig. 14). Also, a ground truth sample polygon (Fig. 13) was simulated and measured using RTK technique. The relative mean error percentage of measurement for the landslide polygon tested in area is 0.496 (i.e., the proposed algorithm in MATLAB vs. ground truth measurement) and 0.43 (i.e., ArcGIS vs. ground truth measurement).

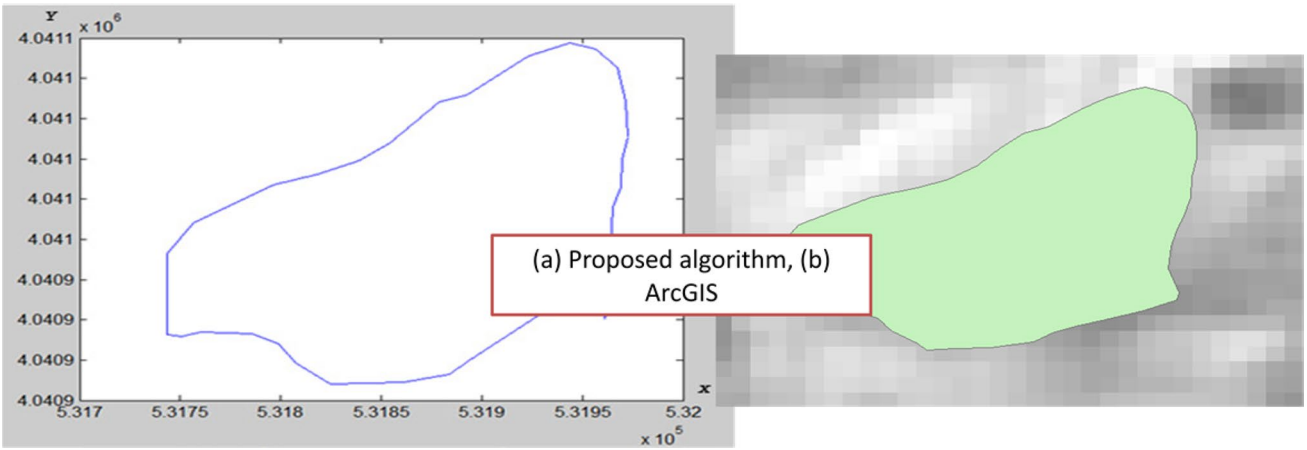

Fig. 14 Representing a landslide polygon automated calculation using **a** the proposed algorithm in MATLAB and **b** ArcGIS

These results showed that the developed algorithm can calculate the length, width, and area of landslide polygons.

Moreover, this study indicated that the LiDAR-derived DEM (Fig. 15) plays an important role to support enhancing landslide on screen visualization to determine a landslide polygon boundary and to revise landslide inventory. This method also helps in determining the length, the width, and particularly the area of landslide polygons when integrating such DEM with the UAV and Google Earth high-resolution images. To support the output results, this study has compared the selected landslide to inventory data and the ground truth observations (Fig. 16). However, this study has not attempted a quantitative research on accuracy performance of the output results. It would be suggested for the future works to compare a quantitative study on the output result by the proposed algorithm and available inventory data. Finally, the proposed method can semi-automatically determine and classify the landslide type from the landslide inventory database.

Conclusion and recommendation

This study has presented a method to define the landslide polygon in a 2D scalar Cartesian coordinate system. The landslides can be classified based on geographic coordinates (x,y), long side or maximum distance of the segment in a landslide polygon, and slope angle (θ). This study has implemented geometric calculation and landslide classification through NITR-based MATLAB coding. The study concluded that the proposed method can discern the length and width of a landslide at a satisfactory level for any landslide polygon shapes. In general, we have regular and irregular shapes. Regular shapes are shapes such as rectangle, triangle, and square. Regular shapes have sides that are all equal and interior (inside) angles that are all equal. Irregular shapes have sides and angles with any length and size. We have landslides that are in various shapes in nature. That is why, this study presumed they can be in regular shape such as a rectangle or they can have an irregular shape.

This study also concluded that use of the LiDAR-derived DEM together with UAV images and Google Earth images can possibly not only improve visual interpretation and recognition of landslides, but also increase the performance in measurements of landslide geometry when integrated with field observations. Therefore, this approach can be used to revise and update the landslide inventory in the study area. This study also identified that the majority of landslides in the study area are rhombic or hexagonal, trapezoid, and oriented to the downslope direction of the hillslope. Also, this study found that the round-shaped landslides are associated with highly dense vegetation. The field observation showed that in a few cases, the material movement and displacement are towards the bed and strata dip direction of the rocks.

The findings of this study suggest that the flow direction or aspect value of mass displacement should be considered for determining landslide type in future studies. Also, the failure direction and slope direction in the 3D vector system and dynamic environment (before and after a landslide) should be considered when determining the deformation, materials displacement, and flow direction. Given the fact that the algorithm developed in this study was not able to accurately identify the right direction or aspect value, a logic relationship should be defined. Further development is required for computing the volume of material displacement using a high-resolution LiDAR-derived DEM and UAV images obtained before and after landslides.

However, this 2D scalar static approach possibly can be used in disaster planning and management and responses when required. The results of this research could also possibly motivate researchers to begin a new

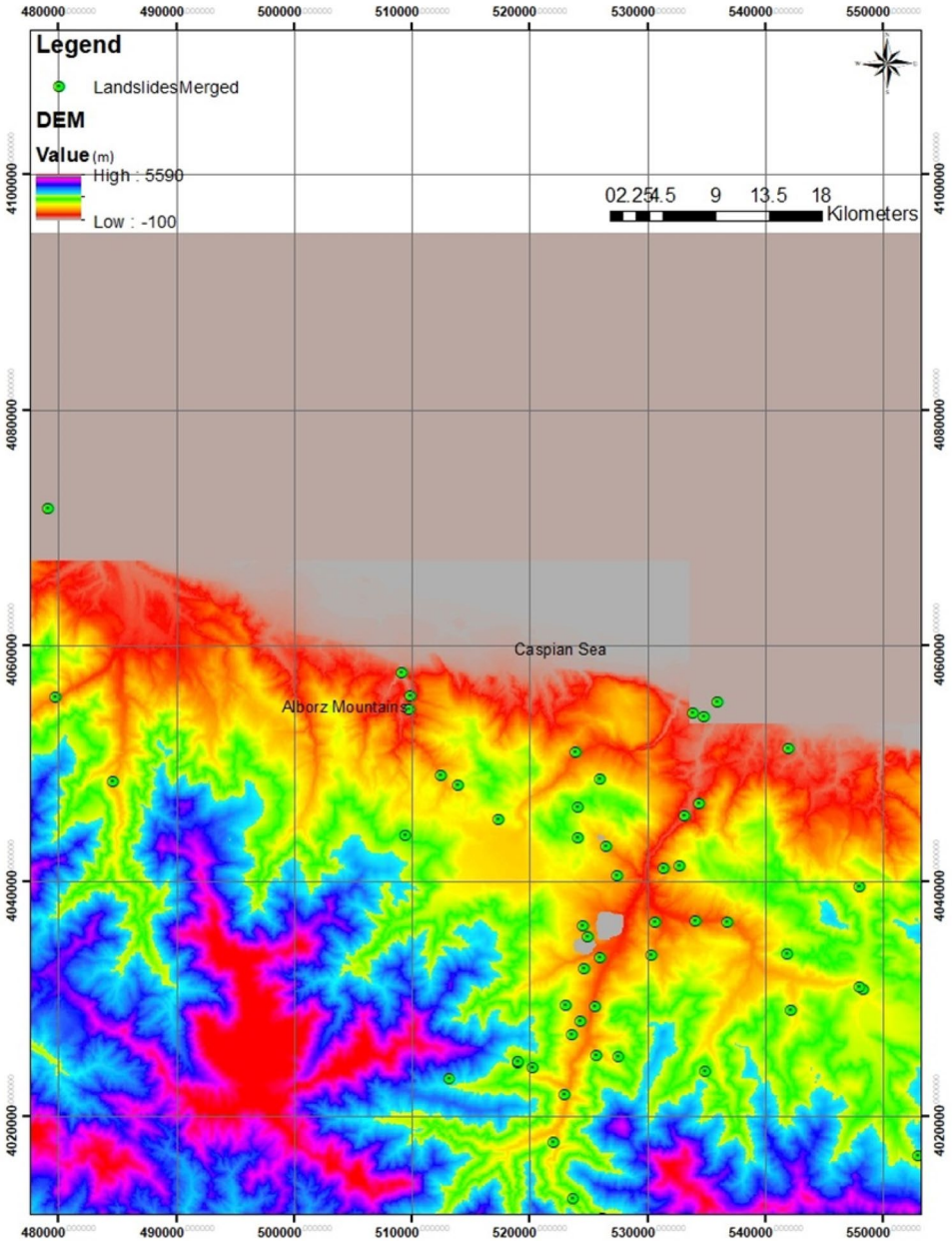

Fig. 15 Landslide inventories on the DEM of the study area

driving point in developing algorithms for automatic geomorphometric analysis of landslides in the GIS environment toward this future direction delivered by the UN-GGIM (http://ggim.un.org/).

Code availability

The MATLAB stat code of the script which implements the algorithm is available at http://www.widm.ca and upon request at s2pirat@uwaterloo.ca.

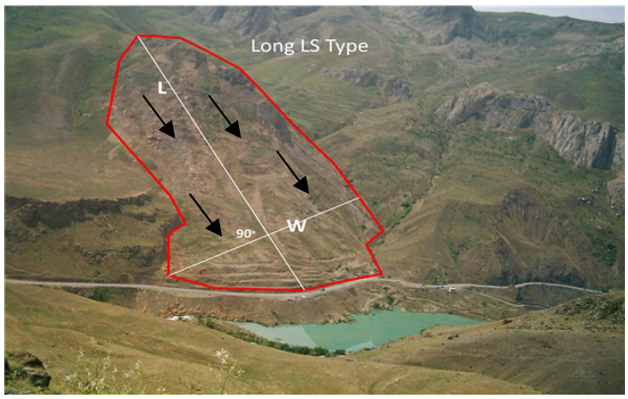

Fig. 16 Field photo shows a long landslide type with length and width segments. Location: Haraz district, Mazandaran Province

Acknowledgements This paper identified the geometric process to determine landslide length, width, area, and type by developing the proposed algorithm. Remote sensing data such as LiDAR are useful to improve the enhancement of determining landslide boundary polygons, geometric analysis, particularly when a high-resolution DEM is acquired. The contribution of this study is on automated geometric and classification of landslides. This contribution allows to do the necessary action for emergency response and disaster planning and management after a landslide occurrence, because we can do geometry calculation immediately by implementing DEMs of before and after a landslide associated with high-resolution of UAV and satellite images. This study aimed to introduce an approach to landslide geometry analysis and classification for future GIS techniques. This study perhaps predicts that future geodata analytical and numerical approaches will be explored more in depth for geometric analysis using UAV for landslide studies. This study delivered a geodata analytical and numerical method for landslide analysis and classification. Now, could researchers incorporate this accurate high-resolution DEM and UAV images in conjunction with inventory dataset and geometric analysis to develop a better modeling and simulation of landslide mechanisms? Is it possible to integrate the proposed algorithm to early warning systems? This study delivered a new geodata analytical and numerical method for landslide geometric analysis and classification. I am thankful to Dr. Seyed Ali Ashrafizadeh, the Visiting Professor of the University of Waterloo for his reflections in writing the script. I also appreciate Mr. Afshin Vaseie Nasrabadi for his valuable comments and for providing me the landslide inventory data.

Funding This work does not have any funding.

Compliance with ethical standards

Conflict of interest The authors do not have any potential conflict of interest.

References

Ali SA, Pirasteh S (2004) Geological applications of Landsat Enhanced Thematic Mapper (ETM) data and Geographic Information System (GIS): mapping and structural interpretation in south-west Iran, Zagros Structural Belt. Int J Remote Sens 25(21):4715–4727

Ali SA, Rangzan K, Pirasteh S (2003a) Remote Sensing and GIS study of tectonics and net erosion rates in the Zagros Structural Belt, southwestern Iran. GISciences Remote Sens 40(4):253–262

Ali SA, Kazem R, Pirasteh S (2003b) Use of digital elevation model for study of drainage morphometry and identification stability and saturation zones in relations to landslide assessments in parts of the Shahbazan area. SW Iran Cartogr 32(2):71–76

Ardizzone F, Cardinali M, Carrara A, Guzzetti F, Reichenbach P (2002) Impact of mapping errors on the reliability of landslide hazard maps. Nat Hazards Earth Syst Sci 2:3–14. https://doi.org/10.5194/nhess-2-3-2002 2002.

Ardizzone F, Cardinali M, Galli M, Guzzetti F, Reichenbach P (2007) Identification and mapping of recent rainfall-induced landslides using elevation data collected by airborne Lidar. Nat Hazards Earth Syst Sci 7:637–650. https://doi.org/10.5194/nhess-7-637-2007

Barlow J, Martin Y, Franklin S (2003) Detecting translational landslide scars using segmentation of Landsat ETMC and DEM data in the northern Cascade Mountains, British Columbia. Can J Remote Sens 29:510–517. https://doi.org/10.5589/m03-018

Booth AM, Roering JJ, Perron JT (2009) Automated landslide mapping using spectral analysis and high-resolution topographic data: Puget Sound lowlands, Washington, and Portland Hills. Oregon Geomorphol 109:132–147

Burden RL, Faires JD (2011) Numerical analysis, 9th edn, Brooks/Cole, Cengage Learning, Boston, p 872

Cruden DM (1991) A simple definition of a landslide. Bull Int Assoc Eng Geol 43:27–29

Dikau R, Brunsden D, Schrott L, Ibsen M-L (eds) (1996) Landslide recognition. Identification, movement and causes. Wiley, Chichester

Freeman GT (1991) Calculating catchment areas with divergent flow based on a regular grid. Comput Geosci 17:413–422. https://doi.org/10.1016/0098-3004(91)90048-I

Gaidzik K, Ramírez-Herrera MT, Bunn M,. Leshchinsky BA, Olsen M, Regmi NR (2017) Landslide manual and automated inventories, and susceptibility mapping using LIDAR in the forested mountains of Guerrero, Mexico. Geomat Nat Hazards Risk 8(2):1054–1079

Ghuffar S, Szekely B, Roncat A, Pfeifer N (2013) Landslide displacement monitoring using 3D range flow on airborne and terrestrial LiDAR data. Remote Sens 5:2720–2745. https://doi.org/10.3390/rs5062720

Golovko D, Roessner S, Behling R, Kleinschmit B (2017) Automated derivation and spatio-temporal analysis of landslide properties in southern Kyrgyzstan. Nat Hazards 85(3):1461–1488

Hattanji T, Moriwaki H (2009) Morphometric analysis of relic landslides using detailed landslide distribution maps: implications for forecasting travel distance of future landslides. Geomorphology 103(3):447–454

Hungr O, Leroueil S, Picarelli L (2014) The Varnes classification of landslide types, an update. Landslides 11(2):167–194

Hutchinson JN (1988) General Report: Morphological and geotechnical parameters of landslides in relation to geology and hydrogeology. In: Proceedings, fifth international symposium on landslides (Ed: Bonnard C), vol 1. Rotterdam: Balkema, pp 3–35

Jaboyedoff M, Thierry O, Abella´n A, Marc-Henri D, Loye A, Metzger R, Pedrazzini A (2012) Use of LIDAR in landslide investigations: a review. Nat Hazards 61:5–28. https://doi.org/10.1007/s11069-010-9634-2

Kreyszig E, Kreyszig H, Norminton EJ (2011) Advanced engineering mathematics, 10th edn. Wiley, New York

Lyons NJ, Mitasova H, Wegmann KW (2014) Improving mass wasting inventories by incorporating debris flow topographic signatures. Landslides 11:385–397. https://doi.org/10.1007/s10346-013-0398-0

Malamud BD, Turcotte DL, Guzzetti F, Reichenbach P (2004) Landslide inventories and their statistical properties. Earth Surf Proc Land 29:687–711. https://doi.org/10.1002/esp.1064

Martha TR, Kerle N, Jetten V, Van Westen CJ, Vinod Kumar K (2010) Characterising spectral, spatial and morphometric properties of landslides for semi-automatic detection using object-oriented methods. Geomorphology 116:24–36. https://doi.org/10.1016/j.geomorph.2009.10.004

McKean J, Roering J (2003) Objective landslide detection and surface morphology mapping using high-resolution airborne laser altimetry. Geomorphology 57:331–351 **(2004)**

Mondini AC, Guzzetti F, Reichenbach P, Rossi M, Ardizzone F (2011) Semi-automatic recognition and mapping of rainfall induced shallow landslides using optical satellite images. Remote Sens Environ 115:1742–1757. https://doi.org/10.1016/j.rse.2011.03.006

Niculiťa M (2016) Automatic landslide length and width estimation based on the geometric processing of the bounding box and the geomorphometric analysis of DEMs. Nat Hazards Earth Syst Sci 16:2021–2030. https://doi.org/10.5194/nhess-16-2021-2016

Niculiță M (2015) Automatic extraction of landslide flow direction using geometric processing and DEMs. Geomorphometry Geosci 10(12):201–203

Petschko H, Bell T, Glade R (2016) Effectiveness of visually analyzing LiDAR DTM derivatives for earth and debris slide inventory mapping for statistical susceptibility modeling. Landslides 13(5):857–872

Picke RJ (1988) The geometric signature: quantifying landslide-terrain types from Digital Elevation Models. Math Geol 20:491–511. https://doi.org/10.1007/BF00890333

Pirasteh S (2018) Landslide Geoanalytics Using LiDAR-derived Digital Elevation Models. University of Waterloo. Canada. Ph.D. thesis. P.149

Pirasteh S, Li J (2016) Landslides investigations from geoinformatics perspective: quality, challenges, and recommendations. Geomat Nat Hazards Risk. https://doi.org/10.1080/19475705.2016.1238850

Pirasteh S, Li J (2017) Probabilistic frequency ratio (PFR) model for quality improvement of landslides susceptibility mapping from LiDAR point clouds. Geoenviron Disaster 4:19. https://doi.org/10.1186/s40677-017-0083-z

Pirasteh S, Woodbridge K, Rizvi SM (2009) Geo-information technology (GiT) and tectonic signatures: the River Karun and Dez, Zagros Orogen in south-west Iran. Int J Remote Sens 30(1–2):389–404

Pirasteh S, Pradhan B, Safari H (2011) Coupling of DEM and remote sensing based approaches for semi-automated detection of regional geo-structural features in Zagros Mountain, Iran. Arab J Geosci. https://doi.org/10.1007/s12517-011-0361-0

Pirasteh S, Li J, Attarzadeh I (2015) Implementation of the damage index approach to rapid evaluation building resistance for earthquake. Earth Sci Inform 8(4):751–758. https://doi.org/10.1007/s12145-014-0204-0

Pirasteh S, Li J, Chapman M (2017) Use of LiDAR-derived DEM and a stream length-gradient index approach to investigation of landslides in Zagros Mountains, Iran. Geocarto J. https://doi.org/10.1080/10106049.2017.1316779

Pradhan B, Pirasteh S (2010) Comparison between prediction capabilities of neural network and fuzzy logic techniques for landslide susceptibility mapping. Disaster Adv 3(2):19–25

Schulz William H (2007) Landslide susceptibility revealed by LIDAR imagery and historical records. Seattle Wash Eng Geol 89:67–87

Sherrod BL, Brocher TM, Weaver CS, Bucknam RC, Blakely RJ, Kelsey HM, Nelson AR, Haugerud R (2004) Holocene fault scarps near Tacoma. Wash USA Geol 32(1):9–12

Shirzadi A, Bui DT, Pham BT, Solaimani K, Chapi K, Kavian A, Shahabi H, Revhaug I (2017) Shallow landslide susceptibility assessment using a novel hybrid intelligence approach. Environ Earth Sci 76:60

Su JG, Bork EW (2006) Influence of vegetation, slope and LiDAR sampling angle on DEM accuracy. Photogramm Eng Remote Sens 72:1265–1274

Su WJ, Stohr C (2000) Aerial photo interpretation of landslides along the Ohio and Mississippi Rivers. Environ Eng Geosci VI(4):311–323

Taylor FE, Malamud BD (2012) The statistical distributions of landslide length to width ratios. Geophysical research abstracts 14, EGU2012-826, 2012 EGU General Assembly 2012

Taylor E, Malamud D, Witt A (2015) What shape is a landslide? Statistical Patterns in landslide length to width ratio, Geophysical research abstracts. 17, EGU2015-10191, 2015. EGU General Assembly

Teza G, Galgaro A, Zaltron N, Genevois R (2007) Terrestrial laser scanner to detect landslide displacement fields: a new approach. Int J Remote Sens 28:3425–3446. https://doi.org/10.1080/01431160601024234

Tian Y, XiaO C, Liu Y (2008) Effects of raster resolution on landslide susceptibility mapping: a case study of Shenzhen. Science in China 51(Suppl 2):188–198

Travelletti J, Oppikofer T, Delacourt C, Malet J, Jaboyedoff M (2008) Monitoring landslide displacements during a controlled rain experiment using a long-range terrestrial laser scanning (TLS). Int Arch Photogramm Remote Sens 37(B5):485–490

Varnes DJ (1978) Slope movement types and processes. In: Schuster RL, Krizek RJ (eds) Special report 176: landslides: analysis and control. Transportation and Road Research Board, National Academy of Science, Washington D.C., pp 11–33

Watts P (2004) Probabilistic predictions of landslide tsunamis off Southern California. Mar Geol 203:281–301

Wehr A, Lohr U (1999) Airborne laser scanning: An introduction and overview. ISPRS J Photogramm Remote Sens 54:68–82

Wen F, Xin S, Cao WY, Zheng B (2017) Landslide susceptibility assessment using the certainty factor and analytic hierarchy process. J Mt Sci 14(5):906–925

Westen CJ, Van CE, Kuriakose SL (2008) Spatial data for landslide susceptibility, hazard, and vulnerability assessment: an overview. Eng Geol 102:112–131

Wu W, Sidle RC (1995) A distributed slope stability model for steep forested watersheds. Water Resour Res 31:2097–2110

Wu S, Li J, Huang GH (2008) Study on DEM-derived primary topographic attributes for hydrologic applications: sensitivity to elevation data resolution. Appl Geogr 28:210–223

Yilmaz I (2010) The effect of the sampling strategies on the landslide susceptibility mapping by conditional probability (CP) and artificial neural network (ANN). Environ Earth Sci 60:505–519

Yousef AM, Pourghasemi HR, El-Haddad BA, Dhahry BK (2015) Landslide susceptibility maps using different probabilistic and bivariate statistical models and comparison of their performance at Wadi Itwad Basin, Asir Region, Saudi Arabia. Bull Eng Geol Environ 75:63–87

Zare M, Pourghasemi HR, Vafakhah M, Pradhan B (2013) Landslide susceptibility mapping at Vaz Watershed (Iran) using an artificial neural network model: a comparison between multilayer perceptron (MLP) and radial basic function (RBF) algorithms. Arab J Geosci 6:2873–2888

Zhao W, Zhang Z (2014) Derivative-Based Trapezoid Rule for the Riemann-Stieltjes Integral. Math Probl Eng. 2014:6. https://doi.org/10.1155/2014/874651**(Article ID 874651)**

Zhou G, Esaki T, Mitani M, Xie M, Mori J (2003) Spatial probabilistic modelling of slope failure using integrated GIS Monte Carlo simulation approach. Eng Geol 68:373–386